EEG Signal Processing for Brain–Computer Interfaces

Chapter · January 2014
DOI: 10.1007/978-3-642-30574-0_46

4 authors, including:

Petia Georgieva
University of Aveiro
87 PUBLICATIONS **450** CITATIONS
SEE PROFILE

Mariofanna Milanova
University of Arkansas at Little Rock
158 PUBLICATIONS **467** CITATIONS
SEE PROFILE

Nikola Kirilov Kasabov
Auckland University of Technology
609 PUBLICATIONS **9,721** CITATIONS
SEE PROFILE

46. EEG Signal Processing for Brain–Computer Interfaces

Petia Georgieva, Filipe Silva, Mariofanna Milanova, Nikola Kasabov

This chapter is focused on recent advances in electroencephalogram (EEG) signal processing for brain computer interface (BCI) design. A general overview of BCI technologies is first presented, and then the protocol for motor imagery noninvasive BCI for mobile robot control is discussed. Our ongoing research on noninvasive BCI design based not on recorded EEG but on the brain sources that originated the EEG signal is also introduced. We propose a solution to EEG-based brain source recovering by combining two techniques, a sequential Monte Carlo method for source localization and spatial filtering by beamforming for the respective source signal estimation. The EEG inverse problem is previously studded assuming that the source localization is known. In this work for the first time the problem of inverse modeling is solved simultaneously with the problem of the respective source space localization.

46.1 Overview

Current computer input devices require some physical contact between the user and the input device, for example, a keyboard, mouse, or trackball. Other interfaces might include speech recognition to allow computer tasks and dictation to be performed by the user without any physical contact. Despite the wide range of computer input devices, it is clear that there may be circumstances where such devices are not suitable. For example, if the user has a motor-control disorder both speech and physical input may be impossible. This is how the idea of a brain computer interface (BCI) emerged, as an alternative communication channel between the human being and the external world. The objective is to record the brain activity variations associated with a thought or mental state and *translate* them into some kind of actuation or command over a target output. Examples of possible uses for such an interface are control of a robot arm, wheelchair movement or writing on a monitor (BCI as a mental keyboard). Among various potential applications, prosthetic limb control is currently a major targeted application, allowing a paralyzed patient to gain motor ability in a BCI controlled limb. Potential users include those with severe head trauma or spinal cord injuries, as well as people with amyotrophic lateral sclerosis (ALS, or Lou Gehrig's disease), cerebral palsy, or other motor-control disorders. BCIs could be useful even for people with lesser, or no, motor impairment, as, for example, computer gamers.

This chapter will present recent advances towards the development of BCI systems that analyze the brain activity of a subject measured through the electroen-

cephalogram (EEG). The work begins with a general overview of BCI technologies, which is followed by a more comprehensive analysis of the EEG-based BCI paradigms. Next, we focus on the main signal processing challenges – EEG signal enhancement, feature extraction, and classification. Finally, we introduce our ongoing research on EEG source estimation by particle filters.

46.2 BCI Technologies

There are three main BCI technologies, which are invasive, partially invasive, and noninvasive. The *invasive BCIs* are based on detection of single neuron activity by intra-cortical electrodes implanted into the gray matter of the brain. Much of the related research has been done with animals (mainly rats and monkeys), although some tests with humans have also been done. For example, successful attempts were reported with patients who already have the electrodes from epilepsy monitoring trials. *Partially invasive BCIs* are based on recording of electrocorticographic (ECoG) implants inside the skull but outside the gray matter. Invasive and partially invasive BCIs are more reliable and less noisy, however implant placement by neurosurgery is required, which brings hardware and ethical problems. For example, important issues concerning the implant suitability for long-term use or their periodical replacement have still to be solved.

Noninvasive BCIs rely on recording of the brain activity at a macro level (in contrast to the single neuron level by invasive BCIs) using various noninvasive techniques. The most typical noninvasive BCI designs use an EEG to measure the potential difference between electrodes placed on the head surface. The EEG machine is a standard medical imaging device and has many advantages: it is safe, cheap, and relatively easy to use. Moreover, the subject preparation for experiments and the recordings are fast and, therefore, it is possible to perform real-time analysis of EEG components.

Alternative noninvasive BCI techniques such as magnetoencephalography (MEG) [46.1], functional magnetic resonance imaging (fMRI) [46.2], and functional near-infrared systems (fNIR) [46.3] are also subject of intensive research. In Fig. 46.1 time versus spatial resolutions of different techniques for brain imaging and the associated hardware complexity and price are depicted. Note that while the EEG technique has a temporal resolution similar to the real neuron activity (in the range of 1 ms), its spatial resolution is the worst among all techniques. Single photon emission computerized tomography (SPECT) and positron emission tomography (PET) do not provide resolution advantages and, additionally, they are more expensive, and therefore they have not yet been reported as BCI technologies. Note that fMRI has the closest spatial resolution to the real neuron activity (around 1 mm^3). However, current technologies for recording MEG and fMRI are expensive, making them not quite practical for wider applications in the near future. fNIR is potentially cheaper but both fMRI and fNIR are based on changes in cerebral blood flow, which has an inherently slow response. Therefore, EEG signal processing is currently the most practical technology for BCI. Nevertheless, building a hybrid BCI that combines the two modalities, EEG and fMRI, and thus benefits from their respective favorable resolutions is an appealing still unexplored alternative.

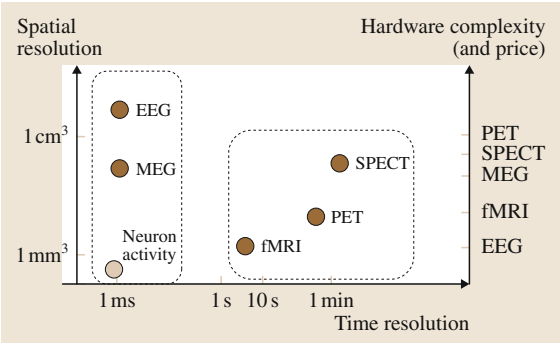

Fig. 46.1 Brain imaging techniques

BCI Sensors

The evolution over time of the electrical sensors used in BCI systems is summarized in Fig. 46.2a. The first BCI system was developed in 1977 by *Jacques Vidal* [46.4] and was based on visual evoked potentials (VEP). The real-time analysis of EEG signals suggested the use of waveform activity in the timeframe of N100–P200 components, with N and P indicating negative and positive peaks, and the numbers indicating the approximate latency in msec. Vidal's achievement was a proof of concept demonstration. Due to the limited computer processing capacity at that time (an XDS

Sigma 7 computer controlled the experiments and an IBM360 mainframe digitized the data) it was far from being practical. Online removal of ocular artifacts was also included in Vidal's system. A decade earlier, *Edmond Dewan*, 1967 [46.5], showed that subjects could learn to transmit Morse code messages using eye movements to modulate their brain waves.

Since 1992 experiments with invasive electrodes (ECoG and intra-cortical) have been performed in the BCI framework, mainly with animals (Fig. 46.2c). However, due to the high risk and hardware and ethical problems, invasive brain imaging is still less implemented. The noninvasive sensors (Fig. 46.2b) evolved from the classical EEG gel-based electrodes, through the near-IR electrodes, and very recently dry electrodes appeared on the market.

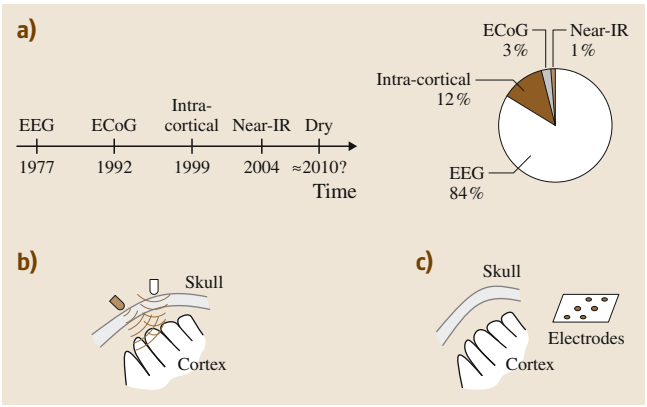

Fig. 46.2 (**a**) BCI electrodes technology evolution; (**b**) noninvasive BCI electrodes; (**c**) invasive BCI electrodes; BCI sensors

46.3 EEG-Based BCI

46.3.1 EEG Waves

The concept of interfacing a computer directly to the brain is a relatively new one, but analysis of brain waves has been reported since 1929 when Hans Berger first recorded EEG signals from a human source using electrodes and a galvanometer. This measured the potential difference between the electrodes placed on the scalp and a reference electrode, placed on the earlobe. The potential difference fluctuations gave an indication to the small current produced by the billions of neurons in the brain when they fire. The combination of the neurons firing in the brain can yield signals that are extremely complex but that have identifiable patterns based upon the activity in the brain. For example, sleeping will produce a substantially different EEG signal to that of a brain computing complex mathematical problems – this can be seen by performing a frequency analysis of the signals. The key concept for BCI designs is the frequency band segmentation. The EEG signal is composed of waves inside the 0–60 Hz frequency band. Different brain activities and states can be identified based on the extracted frequency content of the recorded oscillations [46.6]. The main frequency bands of the EEG signal are listed in Fig. 46.3.

Delta waves (below 4 Hz) are associated with deep sleep. They are a high-amplitude, low-frequency wave and are generated by the lack of processing by neurons. Delta waves can also be found when examining a comatose patient.

Theta waves (4–8 Hz) are typical for dreamlike states and old memories, but can also be associated with anxiety, epilepsy, and traumatic brain injury.

The alpha band (8–13 Hz) corresponds to a relaxed state recorded in the occipital brain zone. The amplitude of alpha waves ranges between 10 and 50 mV.

Sensorimotor (mu) rhythms (8–12 Hz) are associated with the sensory-motor cortex and can be used to recognize intention or preparation of movement and also imaginary motor movement.

Beta (13–30 Hz) waves are associated with alertness, arousal, concentration, and attention. Beta waves are fast but of low amplitude.

The gamma band (30–50 Hz) is characteristic for mental activities such as perception, problem solving, and creativity.

Note that the alpha band and mu-rhythms cover the same frequency range, however, the respective waves are clearly identified at different brain zones.

For each particular brain activity there is one particular area that produces stronger electrical activity in one of the previously referred to frequency bands; similarly, internal artifacts are more relevant in some parts of the scalp than in others. Consequently, EEG signals are multi-channel signals, were each channel corresponds to a specific scalp location. The occipital area of the scalp is known to provide stronger electrical signals in

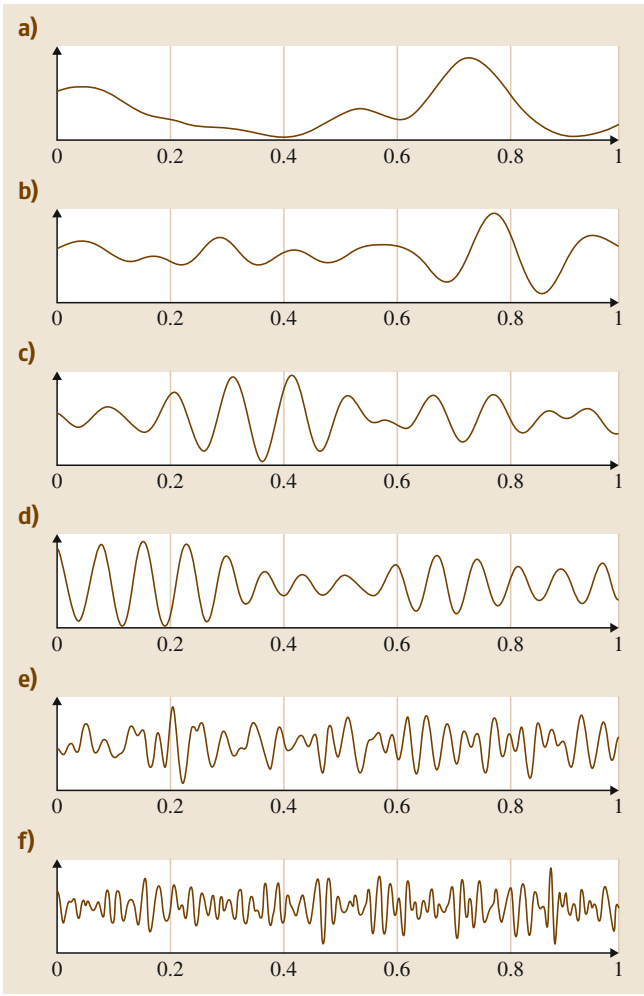

Fig. 46.3a–f EEG waves. **(a)** Delta band (below 4 Hz); **(b)** theta band (4–8 Hz); **(c)** alpha band (8–13 Hz); **(d)** mu-rhythm (8–12 Hz); **(e)** beta band (13–30 Hz); **(f)** gamma band (30–50 Hz)

the band in response to visual stimulation and perception of images.

46.3.2 EEG-Based BCI Paradigms

Among the various noninvasive BCI paradigms proposed, the *sensorimotor* (*mu*) *rhythms* (SMR) and the *visual evoked potentials* (*VEP*) are the most frequently reported.

SMR are spontaneous changes in the EEG oscillations in the 8–12 Hz range registered from the central region of the scalp (sensorimotor cortex) when movement or imagination of movement is performed. At least a second before subjects initiate voluntary movement, the SMR over the hemisphere contralateral to the movement direction decrease in amplitude. SMR activity returns to baseline levels within a second after movement is initiated. These motor activity dependent changes are termed event related desynchronization (ERD) and event related synchronization (ERS). *Wolpaw* et al. [46.7] reported the first use of SMRs for cursor control.

In contrast to spontaneous SMR that do not require special stimuli to occur, VEP changes in the ongoing EEG are generated in response to visual stimulus. However, visual stimuli may comprise different components, such as color, texture, motion, objects, readability (text versus non-text), etc. Each of these components has an impact on the spatial dispersion of the VEP throughout the scalp, being observed differently in each EEG channel. Therefore, to focus the VEP production and analysis, the set of visual stimuli must be coherent, i. e., it should always stimulate the same brain areas. Typical VEP waves are denoted as N100, P100, P200, P300, and N300, with N and P indicating negative and positive peaks and the numbers indicating the approximate latency in milliseconds, for example, P300 stays for positive potentials over 300 ms. Early waves (N100, P100) correspond to perception of sensory stimulus, while latter waves (P300, N300) reflect higher cognitive processes like attention, learning tasks, decision-making, memory, etc. Various studies [46.8–10] showed that VEPs recorded from the human scalp contain a train of short latency wavelets, in the gamma band, precisely time locked to the stimulus and lasting approximately 100 ms. Furthermore, a more recent study [46.11] showed that the perception learning task of a picture set induced neural activity in the gamma band, highly synchronized between occipital electrodes. Finally, the analysis of EEG in response to coherent and noncoherent visual stimulus in a discrimination task evidenced a short-lasting occipital enhancement in the band around 300 ms after stimulus onset in response to coherent images only [46.12].

The most well-known BCI based on VIP is the so-called P300 BCI where a matrix of choices (letters of the alphabet, digits, and other symbols) is presented on screen and the EEG is recorded as these choices flash in succession. The positive potentials around 300 ms after an event significant to the subject is considered a *cognitive* potential since it is generated in tasks where

Table 46.1 BCI feature selection

Extraction method	Time	Frequency	Space	Examples
Time-frequency representation	yes	yes	yes	FT, wavelet
Cell firing rate	yes	yes	yes	—
Power spectral density (PSD)	no	yes	yes	Welch
Pattern matching	yes	no	yes	Correlation
Raw signal	yes	no	yes	Amplitude
Model parameters	yes	no	yes	AR, AAR, KF
Matrix transforms	yes	no	yes	ICA, PCA

the subject discriminates among stimuli. In the P300 spelling device, the subject focuses his/her attention on the desired symbol as the rows and columns of the matrix are repeatedly flashed to elicit VEPs.

An attempt for BCI design based on mental tasks such as solving a mathematical problem, mental counting, and imagining/rotating a 3D object was proposed recently [46.13].

BCI Challenges

Independently of the paradigms discussed above, the main challenges of EEG-based BCIs are related to:

1. The highly nonstationary nature of the EEG signal
2. The low signal to noise ratio (SNR) due to different sources of noise and physiological artifacts
3. Poor spatial resolution.

EEG signals are electric signals gathered at the scalp of an individual. These signals are a combination of signals from two different sources: 1) neural-cerebral activity, called features and 2) noncerebral origins, called artifacts. Internal (physiological) artifacts are artifacts caused by other body activities, such as eye motion, eye blinking, electrocardic activity, and electric activity resulting from muscle contraction. External (environmental) artifacts are artifacts created by external sources, such as power line induction or bad electrode contact. Currently there are many techniques for removing artifacts from EEG signals. Since the original signals received from the electrodes are very weak, in order to generate a useable signal they must be amplified substantially. Therefore, the EEG measurements are subject to pre-processing and filtering to remove the physiological and environmental artifacts and also the background brain activity (for example, jaw clenching) in order to isolate the event related features.

Apart from the EEG signal processing challenges, more technical problems such as effective electrode placement and the required impedance between scalp and electrodes have also been studied. In the past, the EEG was recorded on paper and an impedance of 5 kΩ was required. However, with digital recording of the data it has been found that an impedance of 40 kΩ will still produce usable results.

Further to this, the protocols and drivers of communication between the EEG machine, the computer, and eventually an output device often need special attention. Timing issues represent an additional challenge when real-time control of an external device is the goal of the BCI, as, for example, controlling a wheelchair. Last but not least, the multi-disciplinarity of BCI research requires knowledge and expertise in many different disciplines such as signal processing, computer science, computational neuroscience, and imbedded intelligent systems.

46.3.3 Feature Selection

After amplification and filtering of the row EEG data, the features that define the brain state or activity are selected and extracted. Due to the inherently large EEG signal variability that ranges from session to session for the same subject, through single versus multiple trials also for the same subject, to a clearly expressed

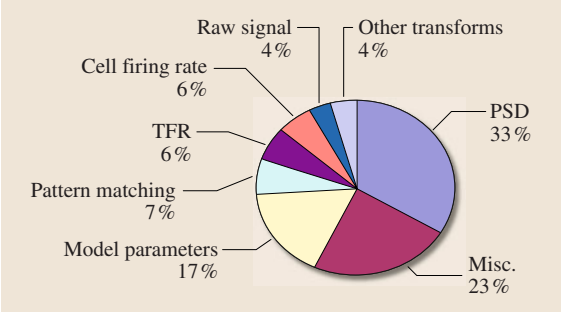

Fig. 46.4 Typical BCI features

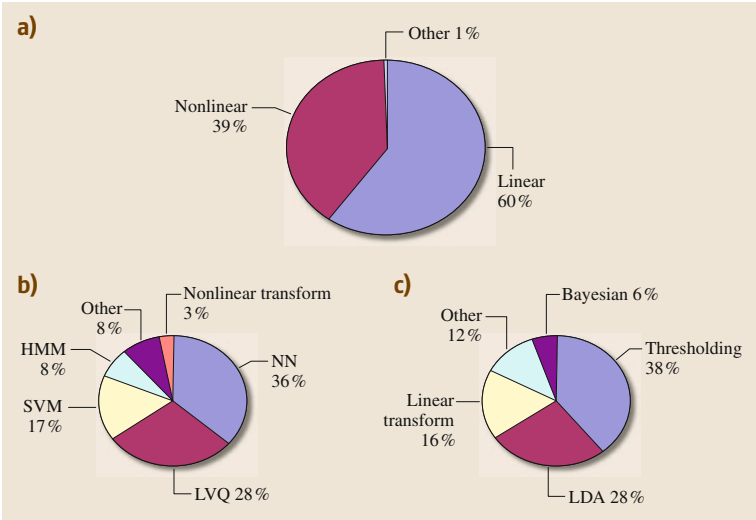

Fig. 46.5a–c Classification techniques for BCI. **(a)** Linear versus nonlinear approaches; **(b)** nonlinear techniques; **(c)** linear techniques

variability from subject to subject, features in time, space, and frequency are defined (see Fig. 46.4 and Table 46.1). The isolation and extraction of the most suitable features of interest is the key for BCI designs and it depends strongly on the BCI paradigm. Through training, the user can learn to control these detectable features.

For BCI-based on motor imagery tasks, SMRs are isolated by the power spectral density (PSD) method. PSD is the most widely applied technique for feature extraction, followed by classical linear methods such as auto regressive (AR) models, adaptive auto regressive (AAR) models, Kalman filtering (KF), and basic matrix transformation such as independent component analysis (ICA) and principal component analysis (PCA).

A combination of various features is an efficient approach to face the higher variability related with VEP BCI.

46.3.4 Classification Techniques

The next step of the BCI design is the feature classification and decoding of the brain state that reflects the subject's desire. The classification approaches are generally devised as nonlinear and linear, the latter being applied more often. The main linear and nonlinear techniques and their respective contribution in the BCI framework are summarized in Fig. 46.5. Among the linear techniques, simple thresholding and linear discriminant analysis (LDA) are generally the best classifiers. As with the nonlinear approach, neural networks (NN), learning vector quantization (LVQ), and nonlinear support vector machines (SVM) are implemented in more than 80% of cases. Although probabilistic techniques like Bayesian classifiers and hidden Markov models (HMM) are very powerful, they need longer execution time (particularly if Monte Carlo runs are required) and, therefore, are not suitable for real-time applications.

46.4 BCI Mobile Robot Control – IEETA Case Study

The protocol for motor imagery BCI designed in the Laboratory of Signal Processing (www.ieeta.pt) by the Institute of Electrical Engineering and Telematics of Aveiro (IEETA) is outlined in this section. The ambulatory EEG device, Trackit system LifeLines Ltd., has eight channels, a sampling frequency of 256 Hz, and a maximum voltage of 10 mV. The electrodes are located according to the standard 10/20 international system (Fig. 46.6) and their size is about 1.5 mm. EEG signals recorded from the central area (C3, C4, Cz), the frontal area (F3, F4), and the parietal area (P3, P4) are used for brain activity decoding.

The objective is to design a communication protocol between the brain and the Khepera mini-robot (5.7 cm diameter) during motor imagery tasks and to successfully control the robot movements over an improvised platform (Fig. 46.7).

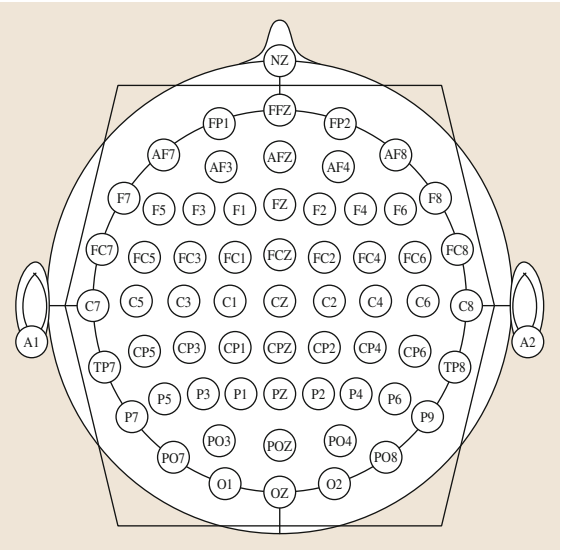

Fig. 46.6 10/20 standard international EEG electrode location system

Before real-time experiments, the user learns to modulate mu-rhythms with the help of visual feedback. The subject is given randomly generated instructions for performing one of the four motor imagery tasks – movements to the right, left, forward, and stopping the screen ball (Fig. 46.8). The BCI classifies the recorded EEG signals and the ball is moved according to the decoded intention.

The algorithm for signal acquisition, pre-processing, feature extraction, and classification of desired commands is summarized next in six steps.

Algorithm 46.1 EEG signal processing for BCI (Fig. 46.9)

Step 1*: *Initialization (fixation period)
Initial period of subject preparation and concentration (3–5 s) during which the personalized baseline EEG signal is recorded.

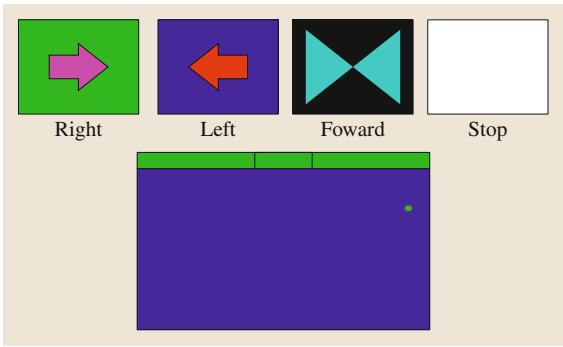

Fig. 46.8 Protocol of subject training

Step 2*: *Standard digital filter
The recorded EEG signals (C3, C4, Cz, P3, P4, F3, F4) are filtered by a standard digital infinite impulse response (IIR) Butterworth filter of the eighth order (1–40 Hz).

Step 3*: *Spatial surface Laplacian filter
For each hemisphere only one corresponding channel is considered obtained by subtracting the mean value of the three neighbor channels:

$$\text{C\_LH} = \text{C3} - 1/3 * (\text{F3} + \text{P3} + \text{Cz}) \quad \text{(left hemisphere)}$$

$$\text{C\_RH} = \text{C4} - 1/3 * (\text{F4} + \text{P4} + \text{Cz}) \quad \text{(right hemisphere)}$$

Step 4*: *Spectral power feature extraction
Sensorimotor (mu) rhythms (8–12 Hz) are extracted from the C_LH and C_RH equivalent signals and divided into segments of 128 sequential samples (0.5 s). The spectral power (P) for each segment per hemisphere is extracted.

***Step 5*: *Event related de-synchronization* (ERD)**
ERD is computed for each channel C_LH and C_RH.

$$\text{ERD\%} = \frac{P - B}{B} 100 \,,$$

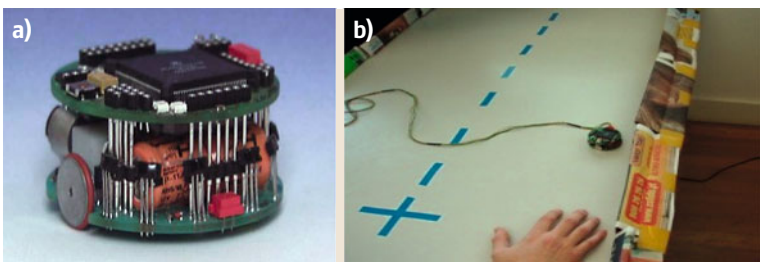

Fig. 46.7 (a) Khepera mini-robot; (b) BCI control of a mobile robot

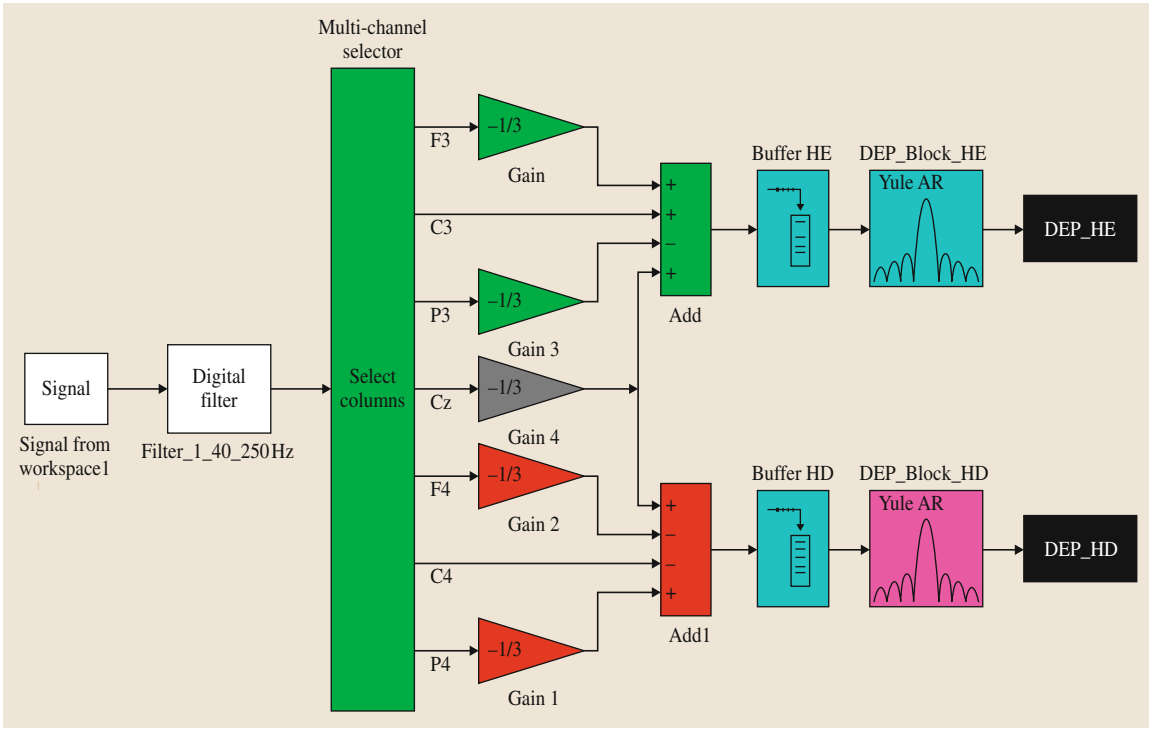

Fig. 46.9 Simulink EEG signal processing

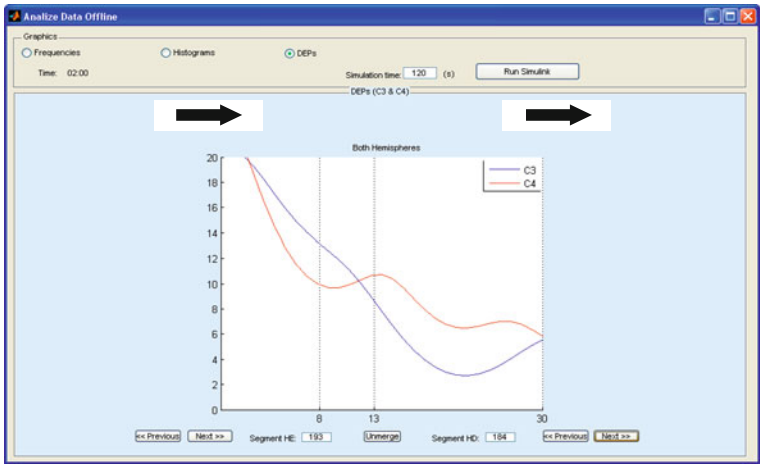

Fig. 46.10 Typical spectral power curves in left (C3) and right (C4) hemispheres related with imagery movement task *to the right*

where B is the mean power value of the baseline signal collected during the fixation period (step 1), P is the spectral power computed during motor imagery tasks (step 4).

Step 6*: *Classification

The classifier has two inputs, one for each ERD block.

Power attenuation is confirmed if ERD has a negative value and the following empirical rules drive the classifier:

- If only the right hemisphere signal verifies the ERD – the classifier output is "LEFT"
- If only the left hemisphere signal verifies the ERD – the classifier output is "RIGHT" (see Fig. 46.10).

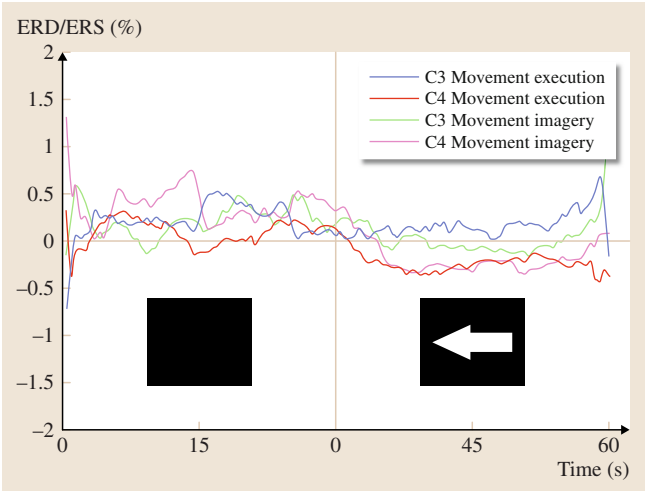

Fig. 46.11 ERD/ERS due to movement imagery versus movement execution ▶

- If both signals verify the ERD – the output is "FORWARD"
- If neither of the signals verify the ERD – the output is "STOP".

In most of the cases studied, the motor imagery BCI can reach an accuracy of up to 70–75%. Other publications report similar results [46.14]. ERD/ERS due to imagination of a physical movement are normally less clearly identifiable compared with ERD/ERS provoked by real movement execution (Fig. 46.11). However, if the subject has some residual motor abilities there exist better human–computer communication techniques than motor imagery BCIs. On the other side, alternatives like VEP BCI are reported to achieve better accuracy; however their technical realization is more difficult and slow, since they require visual stimuli. Moreover, while motor imagery BCI can be automated and the subject can do other cognitive tasks [46.15], P300 BCI requires the total attention of the subject during the stimulus presentation.

46.5 Source-Based BCI

Noninvasive BCI design based not on recorded EEG but on inner brain sources that originated the EEG is called source-based BCI [46.16–19]. The objective of source-based BCI is to find the localization and time patterns of the main brain activity sources by analyzing multichannel EEG recordings. The intuition behind this is that, hopefully, the recovered original sources will be less noisy and thus the essential information can be more reliably decoded. Additionally, we expect to reduce the dimensionality of the problem by extracting a fewer number of dominant sources than the number of surface electrodes.

In brain imaging, EEG source signal estimation is also known as the EEG inverse problem. The problem can be formulated as follows: using the measurements of electrical potential on the scalp recorded from multisensors, the goal is to build a reconstruction system able to estimate the location (the brain area) and the magnitude and directions of the dominative neural brain sources that most probably have originated the recorded EEG signal. Thus the problem can be divided into two stages: 1) *localization of the principal original sources inside the brain* and 2) *estimation of the source signal* (waveforms).

The problem of reconstructing the time pattern of the original source signals from a sensor array, can be expressed as a number of related blind source separation (BSS) problems. *Choi* et al. [46.20] present a review of various BSS and independent component analysis (ICA) algorithms for static and dynamic models in their applications. Beamforming (BF) is also a popular analysis procedure for noninvasively recorded electrophysiological data sets. The goal is to use a set or recording sensors and combine the signals recorded at individual sites to increase the SNR, but focusing on a certain region in space (region-of-interest, ROI). In that sense, beamforming uses a different approach to image brain activities: the whole brain is scanned point by point. Thus, it is, in fact, a spatial filter designed to be fully sensitive to activity from the target location, while being as insensitive as possible to activity from other brain regions. This is achieved by constructing the spatial filter in an adaptive way, i. e., by taking into account the recorded data. More concretely, BF is carried out by weighting the EEG signals, thereby adjusting their amplitudes such as that when added together they form the desired source signal.

In this chapter we propose a solution to the EEG-based brain source recovering by combining two techniques, namely a sequential Monte Carlo (SMC) method for source localization and spatial filtering by BF for the respective source signal estimation based on

EEG measurements. The EEG inverse problem is intensively studded assuming that the source localization is known. In this work, for the first time the problem of inverse modeling is solved simultaneously with the problem of the respective source space localization.

46.5.1 Sequential Monte Carlo Problem Formulation

We consider the problem of the EEG source localization as an estimation problem and solve it within the SMC framework. To define the estimation problem, consider the evolution of the state sequence $\{x_k, k \in \mathrm{N}\}$ of a target given by

$$x_k = f(x_{k-1}, w_{k-1}) , \tag{46.1}$$

where the state x at time k ($x_k \in \Re^{n_x}$) is possibly a nonlinear function f of the state x_{k-1} at the previous time $k-1$ and is also affected by the process noise sequence w_{k-1}; N is the set of natural numbers. The objective is to recursively estimate x_k from measurements

$$z_k = h(x_k, v_k) , \tag{46.2}$$

where h is a possibly nonlinear function and v_k is the measurement noise sequence. Expressions (46.1) and (46.2) are the state and the measurement equations of the general state-space transition model required by the SMC estimation [46.21]. In particular we seek filtered estimates of x_k based on the set of all available measurements up to time k. It is assumed that the observations are taken at discrete time points with a discretization time step T.

Within the Bayesian framework, the estimation problem is to recursively calculate some degree of belief in the state x_k at time k, given the data $z_{1:k}$ up to time k [46.22]. Thus it is required to construct the posterior probability density function (pdf) $p(x_k \mid z_{1:k})$. It is assumed that the initial pdf $p(x_0 \mid z_0) \equiv p(x_0)$ of the state vector, which is also known as the prior, is available (z_0 is the initial measurement). Then, in principle, the posterior conditional pdf $p(x_k \mid z_{1:k})$ may be obtained recursively, in two stages: *prediction* and *update*. Suppose that the required pdf $p(x_{k-1} \mid z_{1:k-1})$ at time $k-1$ is available. The prediction stage involves using the system model (46.1) to obtain the prior pdf of the state at time k via the Chapman–Kolmogorov equation

$$p(x_k \mid z_{1:k-1}) = \int p(x_k \mid x_{k-1}) p(x_{k-1} \mid z_{1:k-1}) \mathrm{d}x_{k-1} , \tag{46.3}$$

since (46.1) describes a Markov process of order one $p(x_k \mid x_{k-1}, z_{1:k-1}) = p(x_k \mid x_{k-1})$. The probabilistic model of the state evolution $p(x_k \mid x_{k-1})$ is defined by the system equation (46.1) and the known statistics of w_{k-1}. At time step k, a measurement z_k becomes available and this may be used to update the prior (update stage) via Bayes' rule

$$p(x_k \mid z_{1:k}) = \frac{p(z_k \mid x_k) p(x_k \mid z_{1:k-1})}{p(z_k \mid z_{1:k-1})} = \frac{\text{likelihood} * \text{prior}}{\text{evidence}} , \tag{46.4}$$

where $p(z_k \mid z_{1:k-1})$ is a normalizing constant defined by the measurement model (46.2) and the known statistics of v_k. Hence, the recursive update of $p(x_k \mid z_k)$ is proportional to

$$p(x_k \mid z_{1:k}) \propto p(z_k \mid x_k) p(x_k \mid z_{1:k-1}) . \tag{46.5}$$

In the update stage (46.4) the measurement is used to modify the prior density to obtain the required posterior density of the current state. The recurrence relations (46.3) and (46.4) form the basis for the optimal Bayesian framework.

In most real-life problems the recursive propagation of the posterior density cannot be performed analytically (the integral in (46.3) is intractable). Usually numerical methods are used and, therefore, a sample-based construction to represent the state pdf. The family of techniques that solve the estimation problem numerically are denoted as particle filtering methods (also known as nonparametric methods). Particle filters (PF) were first defined in the sequential Monte Carlo (SMC) framework and applied to object and video tracking. In the SMC framework, multiple particles (samples) of the state are generated, each one associated with a weight $W_k^{(l)}$ which characterizes the quality of a specific particle l, $l = 1, 2, \ldots, N$. Thus, a set of N weighted particles, drawn from the posterior conditional pdf, is used to map integrals to discrete sums. The posterior $p(x_k \mid z_{1:k-1})$ is approximated by the weighted sum of particles

$$\hat{p}(x_k \mid z_{1:k-1}) = \sum_{l=1}^{N} W_{k-1}^{(l)} \delta\left(x_k - x_k^l\right) , \tag{46.6}$$

and the update probability is

$$p(x_k \mid z_{1:k}) = \sum_{l=1}^{N} \hat{W}_k^{(l)} \delta\left(x_k - x_k^l\right) , \tag{46.7}$$

where

$$W_k^{(l)} = W_{k-1}^{(l)} p(z_k \mid x_k) = W_{\text{previous}} * , \text{likelihood} \tag{46.8}$$

and the normalized importance weights

$$\hat{W}_k^{(l)} = \frac{W_k^{(l)}}{\sum_{l=1}^{N} W_k^{(l)}} \,. \tag{46.9}$$

New weights are calculated, putting more weight on particles that are important according to the *posterior* pdf (46.7). It is often impossible to sample directly from the posterior density function $p(x_k \mid z_{1:k})$. This difficulty is circumvented by making use of the importance sampling from a known *proposal distribution* $p(x_k \mid x_{k-1})$. During the prediction stage each particle is modified according to the state model (46.1). In the update stage, each particle's weight is re-evaluated based on the new data.

Particle Degeneracy Phenomenon

An inherent SMC problem is particle degeneracy, the case when a small set of particles (or even just one particle) have significant weights. An estimate of the measure of degeneracy [46.23] at time k is given as

$$N_{\text{eff}} = \frac{1}{\sum_{l=1}^{N} \left(W_k^{(l)}\right)^2} \,, \tag{46.10}$$

where N_{eff} is the number of (effective) particles with significant weights. If the value of N_{eff} is very low, a resampling procedure can help to avoid degeneracy. A schematic representation of the resampling procedure is depicted in Fig. 46.1. Particles with small weights are eliminated, while particles with large weighs are replaced by a number of particles with smaller weights. There are two alternative mechanisms to schedule the resampling, either resampling at each iteration or resampling when the effective number of particles falls below a user-defined threshold N_{thres}. It is known that resampling reduces the variance of the particle population, making the estimation procedure susceptible to outliers with high importance weights and reducing the ability of the SMC to adapt to rapid changes in the states. Therefore, it is crucial to carefully choose N_{thres} in order to maintain the variety within the particle population and still counteract the tendency of focusing all the weight importance in one particle.

46.5.2 EEG Source Localization Model in State-Space

In order to apply the particle filter, outlined in the previous section, the state-space transition model of the source localization is first defined.

Source Model as a Current Dipole Model

Let us assume brain activity arises at a small zone of the cortex centered at location x_s and that the observation point x is some distance away from this zone. The primary current distribution can be approximated by an equivalent current dipole represented as a point source

$$J^p(x_s) = s\delta(x - x_s) \,, \tag{46.11}$$

where $\delta(x)$ is the Dirac delta function, with moment

$$s \equiv \int J^p(x_s) \mathrm{d}x_s \,. \tag{46.12}$$

The current dipole is an extension of the model of the paired-charges dipole in electrostatics. It is important to note that brain activity does not actually consist of discrete sets of physical current dipoles, but rather that the dipole is a convenient representation for coherent activation of a large number of pyramidal cells, possibly extending over a few square centimeters of gray matter. The current dipole model is the key of EEG processing since a primary current source of arbitrary extent can always be broken down into small regions, with each region represented by an equivalent current dipole.

Assuming that the electrical activity of the brain can be modeled by a number of dipoles, i. e., the measured multi-channel EEG signal signals $z_k \in \Re^{n_z}$ from n_z sensors at time k are produced by M dipoles, the forward EEG model is given by

$$z_k = \sum_{m=1}^{M} L_m(x_k(m)) s_k(m) + v_k \,, \tag{46.13}$$

where $x_k(m)$ is a three-dimensional localization vector (space directions), $L_m(x_k(m)) \in \Re^{n_z \times 3}$ is the lead field matrix for dipole m, $s_k(m)$ is a three-dimensional moment vector of the m-th dipole (the source signal). By v_k the effect of noise in the measurements is simulated. $L_m(x_k(m))$ is a nonlinear function of the dipole localization, electrodes positions, and head geometry, [46.24]. Its three columns contain the activity that will be measured at the sensors due to a dipole source with unity moment in the x-, y-, and z-directions, respectively, and zero moment in the other directions. An analytical expression for the forward model exists if the dipole localization, electrode positions, and head geometry are known. The spherical head model is a simplification that preserves some important electrical characteristics of the head, while reducing the mathematical complexity of the problem. The different electric conductivities of the many layers between the brain and the measuring

surface need to be known. The skull is typically assumed to be more resistive than the brain and scalp that, in turn, have similar conductivity properties [46.25].

In the framework of the dipole source localization problem, the states that need to be estimated are the geometrical positions of M dipoles

$$x_k = [x_k(1), \ldots, x_k(M)] , \quad \text{where}$$
$$x_k(m) = [x(m), y(m), z(m)]^{\mathrm{T}} \quad \text{for } m = 1, \ldots, M . \tag{46.14}$$

Then the lead field matrix of M dipoles $L_m(x_k) \in \Re^{n_z \times 3M}$ is

$$L(x_k) = [L(x_k(1)), \ldots, L(x_k(M))] . \tag{46.15}$$

The vector of moments $s_k \in \Re^{3M \times 1}$ is $s_k = [s_k(1), \ldots, s_k(M)]^{\mathrm{T}}$, where each $s_k(m)$ consists of the brain source signals in each space direction, $s_k(m) = [s_x(m), s_y(m), s_z(m)]^{\mathrm{T}}$.

Equation (46.13) can be reformulated in matrix form as follows

$$z_k = L(x_k)s_k + v_k . \tag{46.16}$$

Expression (46.16) corresponds to the measurement equation (46.2) of the general transition model. As for the state equation (46.1), since it is unknown how the states (the geometrical positions of M dipoles) evolve over time, a random walk model (first-order Markov chain) is assumed in the source localization space,

$$x_k = x_{k-1} + w_k . \tag{46.17}$$

Equations (46.16) and (46.17) define the dipole source localization model in state space. The intuition behind the PF approach is to estimate the 3-D location (vector x) of the principle M dipoles (assuming M is known) that originated the underlying EEG recordings z_k. In the above model certain distributions for the process and the measurement noises are assumed and initial values for the states are chosen. The lead field matrix can then be computed, however the moments $s_k(m)$ are not known. In order estimate them the BF approach is used.

46.5.3 Beamforming as a Spatial Filter

BF deals with the estimation of the time patterns in three space directions of the m-th current dipole $s_k(m) = [s_x(m), s_y(m), s_z(m)]^{\mathrm{T}}$ located at $x_k(m) = [x(m), y(m), z(m)]^{\mathrm{T}}$ using the measurements of electrical potential on the scalp recorded from N sensors located at the surface of the head. The beamformer filter consists of weight coefficients (B) that when multiplied by the electrode measurements give an estimate of the dipole moment at time k

$$s_k = B^{\mathrm{T}} z_k , \tag{46.18}$$

where $B \in \Re^{n_z \times 3M}$ is the weighting matrix. The choice of the beamformer weights is based on the statistics of the signal vector z_k received at the electrodes. Basically, the objective is to optimize the beamformer response with respect to a prescribed criterion, so that the output s contains minimal contribution from noise and interference. There are a number of criteria for choosing the optimum weights. The method described below represents a linear transformation where the transformation matrix is designed according to the solution of a constrained optimization problem (early work on this is attributed to [46.26].

The basic approach consists in the following: assuming that the desired signal and its direction are both unknown, accurate signal estimation can be provided by minimizing the output signal variance. To ensure that the desired signal is passed with a specific (unity) gain, a constraint may be used so that the response of the beamformer to the desired signal is

$$B^{\mathrm{T}} L(x_k) = I , \tag{46.19}$$

where I denotes the identity matrix. Minimization of contributions to the output due to interference is accomplished by choosing the weights to minimize the variance of the filter output

$$\mathrm{Var}\{y_k\} = \mathrm{tr}\{B^{\mathrm{T}} R_{zk} B\} , \tag{46.20}$$

where tr{} is the trace of the matrix in brackets nad R_{zk} is the covariance matrix of the EEG signals. In practice, R_{zk} will be estimated from the EEG signals during a given time window. Therefore, the filter is derived by minimizing the output variance subject to the constraint defined in (46.19). This constraint ensures that the desired signal is passed with unit gain. Finally, the optimal solution can be derived by constrained minimization using Lagrange multipliers [46.27] and it can be expressed as

$$B^{\mathrm{opt}} = R_{zk}^{-1} L^{\mathrm{T}}(x_k) \left(L^{T}(x_k) R_{zk}^{-1} L(x_k) \right)^{-1} . \tag{46.21}$$

The response of the beamformer is often called the linearly constrained minimum variance (LCMV) beamformer. LCMV provides not only an estimate of the source activity, but also its orientation, which is why it is classified as vector beamforming. The differences and similarities among beamformers based on this criterion for choosing the optimum weights are discussed in [46.28].

46.5.4 Experimental Results

In this section we test the algorithm with real EEG data. The solution of the EEG source localization problem requires a significant number of forward model evaluations. The proposed algorithm can require its evaluation at thousands of different source locations. In order to control the computational load, a discrete state-space is assumed, which consists of a finite number of states (dipoles). The dipoles are linearly distributed in a cube with limits $[-9; 9]$ cm. We use a linear grid $(8\times8\times8)$ to generate 512 dipoles. Based on the information for the localization of the grid of brain dipoles and the localization of the surface scalp electrodes the lead field matrix $L(x)$ is computed. The SMC algorithm for EEG source estimation is summarized below. The algorithm was inspired by related previous works [46.29–31].

Algorithm 46.2 Sequential Monte Carlo algorithm for EEG source localization

for run $= 1, 2, \ldots,$ MC
(repeat the same algorithm MC number of runs)

Initialization

I. $k = 0$, **for** $l = 1, 2, \ldots, N$
Generate N samples according to a chosen distribution $x_0^{(l)} \sim p(x_0)$ around the initial vector $x_0 = \min(D) + (\max(D) - \min(D)) * \text{rand}(1, N)$. Set initial weights $W_0^{(l)} = \frac{1}{N}$ (equal initial importance to all samples)
II. **for** $k = 1, 2, \ldots$

Prediction step

For $l = 1, 2, \ldots, N$ compute the state prediction according to the random walk state equation (46.17) $x_k = x_{k-1} + w_k$, where $w_k \sim N(0, Q)$ is the process (assumed Gaussian) noise, $E[w_k w'_{k+j}] = 0$ for $j \neq 0$. The covariance matrix Q of w_k is $Q = \sigma_w^2 I$, I denotes the unit matrix and σ_w is the standard deviation. σ_w is chosen as a percentage (0–50%) from the previously estimated state vector x_{k-1}.

Beamforming step

1. Compute the transfer function $L(x_k)$
2. apply the BF technique to define the spatial filter w using (46.21)
3. compute the amplitudes at time k of the source signal propagated in three directions, for all estimated sources y_k

Measurement Update

Evaluate the importance weights
for $l = 1, 2, \ldots, N$, on the receipt of a new measurement, compute the output according to the measurement equation (46.16) and compute the weights $W_k^{(l)} = W_{k-1}^{(l)} \text{Lic}\left(z_k \mid x_x^{(l)}\right)$
The likelihood is calculated as
$\text{Lic}\left(z_k \mid x_x^{(l)}\right) \sim N\left(h(x_k^{(l)}), \sigma_v\right)$
$\text{Lic}\left(z_k \mid x_x^{(l)}\right) = \exp\left[-0.5 * (z_k - \text{EEG}_{\text{data}\_k}) R^{-1}(z_k - \text{EEG}_{\text{data}\_k})\right]$
$R = \text{cov}(\text{EEG}_{\text{data}}) = (\text{EEG}_{\text{data}})(\text{EEG}_{\text{data}})^{\text{T}} =$
1) **for** $l = 1, 2, \ldots, N$, normalize the weights $\hat{W}_k^{(l)} = W_k^{(l)} / \sum_{l=1}^{N} W_k^{(l)}$

Output

2) Calculate the posterior mean $E[x_k \mid z_{1:k}]$ as $\hat{x}_k = E[x_k \mid z_{1:k}] = \sum_{l=1}^{N} \hat{W}_k^{(l)} x_k^{(l)}$

Compute the effective sample size

$$N_{\text{eff}} = \frac{1}{\sum_{l=1}^{N} \left(\hat{W}_k^{(l)}\right)^2}$$

Selection step (resampling) if $N_{\text{eff}} < N_{\text{tresh}}$

3) Multiply/suppress samples $x_k^{(l)}$ with high/low importance weights $\hat{W}_k^{(l)}$, in order to obtain N new random samples approximately distributed according to the posterior state distribution. The residual resembling algorithm, [46.23] is applied. This is a two-step process making use of sampling-importance-resampling scheme:
for $l = 1, 2, \ldots, N$ set $W_k^{(l)} = \hat{W}_k^{(l)} = \frac{1}{N}$.

It is assumed that the EEG signal has originated by activity in two principal dipoles, hence the dimension of the state vector at each time k is $x_k \in \Re^{6\times1}$ (three coordinates per dipole). The initial state vector $x_0 = [x_{10}, y_{10}, z_{10}, x_{20}, y_{20}, z_{20}]^{\text{T}}$ is chosen randomly

$$\{d_{i0} : [x_{i0} \in [-9;\ 9]\text{cm},\ y_{i0} \in [-9;\ 9]\text{cm},\ z_{i0} \in [9;\ 9]]\text{cm}\}\,, \quad i = 1, 2\,.$$

The number of initially generated particles is $N = 500$ and the complete algorithm is executed 5 times (MC = 5 runs). Increasing N (the same stays also for MC) makes the estimation process rather time-consuming while decreasing N worsen the convergence properties of the algorithm.

The real EEG data correspond to visually evoked potential (VEP) signals extracted from 13 female subjects (20–28 years old). All participants had normal or corrected to normal vision and no history of neurological or psychiatric illness. Neutral, fearful, and disgusting faces of 16 different individuals (8 males and 8 females) were selected, giving a total of 48 different facial stimuli. Images of 16 different house fronts

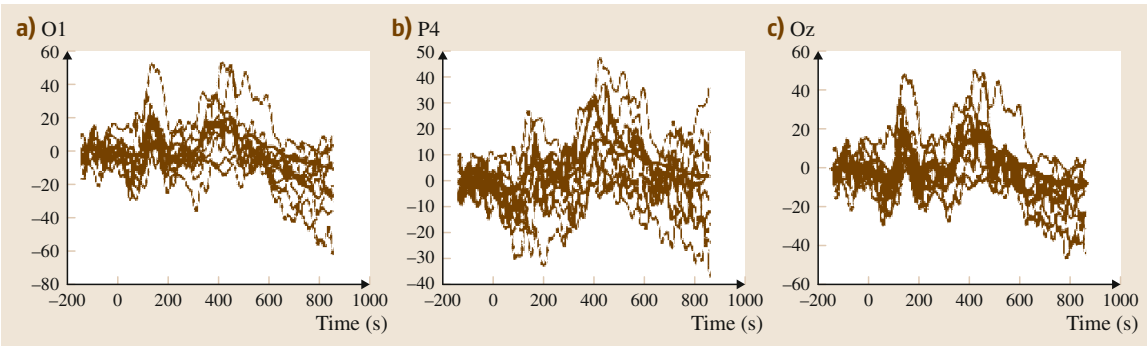

Fig. 46.12a–c Superposition of 10 VEP trials measured at **(a)** O1, **(b)** P4, and **(c)** Oz channels

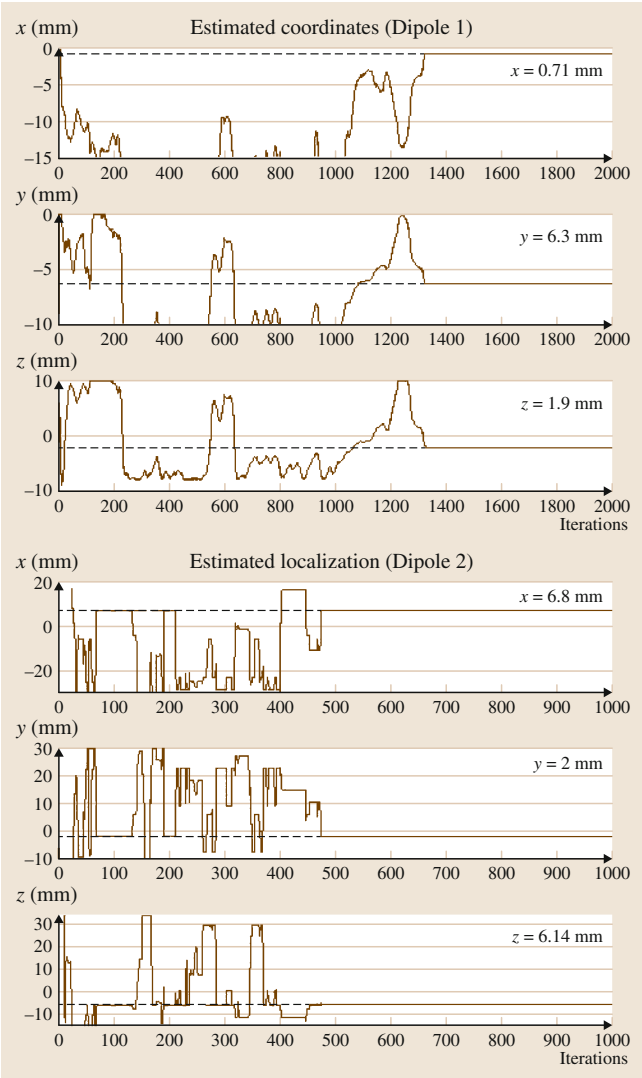

to be superimposed on each of the faces were selected from various internet sources. This resulted in a total of 384 gray scaled composite images (9.5 cm wide by 14 cm high) of transparently superimposed face and house with equivalent discriminability.

Participants were seated in a dimly lit room, where a computer screen was placed at a viewing distance of approximately 80 cm coupled to a PC equipped with software for the EEG recording. The images were divided into two experimental blocks. In the first, the participants were required to attend to the houses (ignoring the faces) and in the other they were required to attend to the faces (ignoring the houses). The participant's task was to determine, on each trial, if the current house or face (depending on the experimental block) was the same as the one presented on the previous trial. Stimuli were presented in sequence, for 300 ms each and were preceded by a fixation cross displayed for 500 ms. The inter-trial interval was 2000 ms.

EEG signals were recorded from 20 electrodes (Fp1, Fp2, F3, F4, C3, C4, P3, P4, O1, O2; F7, F8, T3, T6; P7, P8, Fz, Cz, Pz, Oz) according to the 10/20 international system. EOG signals were also recorded from electrodes placed just above the left supra orbital ridge (vertical EOG) and on the left outer canthus (horizontal EOG). VEP were calculated off-line, averaging segments of 400 points of digitized EEG (12 bit A/D converter, sampling rate 250 Hz).

These segments covered 1600 ms comprising a prestimulus interval of 148 ms (37 samples) and poststimulus onset interval of 1452 ms. Before processing, EEG was visually inspected and those segments with excessive EOG artifacts were manually eliminated. Only trials with correct responses were included in

Fig. 46.13 Estimation of two source locations that produce P100 VEP peak in occipital channels ◀

the data set. The experimental setup was designed by [46.32] for their study on subject attention and perception using VEP signals.

Figure 46.12 represents ten enhanced (by principal component analysis) trials of three channels. In the reconstructed signals it is possible to identify a positive peak in the range of 100–160 ms (P100). P100 corresponds to the perception of the sensory stimulus, a brain activity that is known to happen in the primary visual cortex. The occipital channels (O1, Oz) that measure the brain activity around the visual cortex clearly represent the P100 peaks. The task of the SMC algorithm is to estimate the two strongest sources (d1 and d2) that may have produced the P100. The results of the estimation are summarized in Fig. 46.13. It is very interesting to observe that the final coordinates of d1 (0.71 mm, −6.3 mm, −1.9 mm) and d2 (6.8 mm, −2 mm, −6.14 mm) correspond to the zone of the primary visual cortex as illustrated in Fig. 46.14. Therefore, the proposed beamformer-based SMC successfully estimated the space coordinates of the two strongest brain sources, producing the P100 peak, as located in the zone of the primary visual cortex.

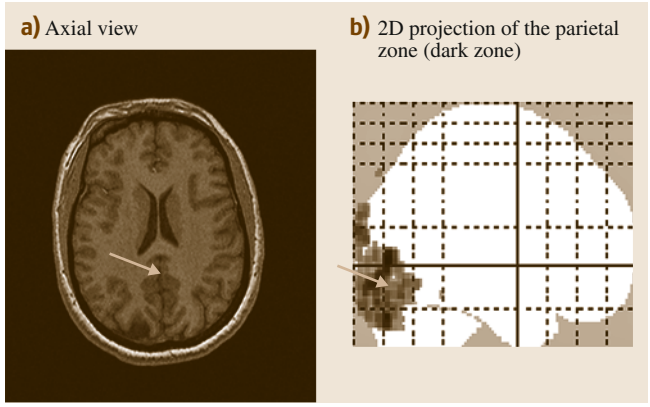

Fig. 46.14a,b Primary visual cortex zone. **(a)** Axial view; **(b)** 2-D projection of the parietal zone (*dark zone*)

46.6 Conclusions

This chapter has described recent efforts towards the development of EEG-based brain computer interface systems. In the first part, motor imagery noninvasive BCI for mobile robot control was discussed. In the second part an introduction to the underlying principles of source-based BCI was given. Different problems in developing BCI systems and in their applications arise when moving from the electrode-based domain to the source-based scale. The goal of the source-based approach is to obtain knowledge about brain activity and to answer fundamental questions about interacting regions. A combination of probabilistic (SMC) and deterministic (BF) techniques was proposed for the estimation of the principal activity zones in the brain, and its potential as a new direction in BCI design was demonstrated. The method requires a priori knowledge about the number of active sources. The insights gained with this study can be relevant when optimizing the design and implementation of practical source-based BCI. However, there are a number of open issues that need to be studied. For example, the problem of the localization and number of measurement electrodes to be used in order to recover the active zones.

Creating a hybrid BCI paradigm where more than one noninvasive modality are combined such as, for example EEG, estimated brain sources, and fMRI seems the most logical continuation of the present research. In order to increase the information transfer rate and reach the accuracy of the invasive brain imaging techniques a multi-modal approach is required.

References

46.1 J. Mellinger, G. Schalk, C. Braun, H. Preissl, W. Rosenstiel, N. Birbaumer, A. Kübler: An MEG-based brain-computer interface, Neuroimage **36**(3), 581–593 (2007)

46.2 R. Sitaram, A. Caria, R. Veit, T. Gaber, G. Rota, A. Kuebler, N. Birbaumer: fMRI brain-computer interface: A tool for neuroscientific research and treatment, Comput. Intell. Neurosci. **2007**, 25487–1–25487–10 (2007), doi:10.1155/2007/25487

46.3 S.M. Coyle, T.E. Ward, C.M. Markham: Brain–computer interface using a simplified functional near-infrared spectroscopy system, J. Neural Eng. **4**, 219–226 (2007)

46.4 J.J. Vidal: Real-time detection of brain events in EEG, Proc. IEEE **65**(5), 633–641 (1977)

46.5 E.M. Dewan: Occipital alpha rhythm eye position and lens accommodation, Nature **214**, 975–977 (1967)

46.6 E. Niedermeyer, F. Lopes da Silva: *Electroencephalography* (Lippincott Williams and Wilkins, Philadelphia 1999)

46.7 J.R. Wolpaw, D.J. McFarland, G.W. Neat, C.A. Forneris: An EEG-based brain-computer interface for cursor control, Electroencephalogr. Clin. Neurophysiol. **78**(83), 252–259 (1991)

46.8 E. Basar: *EEG Brain Dynamics: Relation between EEG and brain evoked potentials* (Elsevier/North-Holland Biomedical, Amsterdam 1980)

46.9 E. Basar, B. Rosen, C. Basar-Eroglu, F. Greitschus: The associations between 40 Hz-EEG and the middle latency response of the auditory evoked potential, Int. J. Neurosci. **33**(1/2), 103–117 (1987)

46.10 R. Galambos: A comparison of certain gamma band (40-Hz) brain rhythms in cat and man. In: *Induced Rhythms in the Brain*, ed. by E. Başar, T.H. Bullock (Birkhäuser, Boston USA 1992) pp. 201–216

46.11 T. Gruber, M.M. Müller, A. Keil: Modulation of induced gamma band responses in a perceptual learning task in the human EEG, J. Cogn. Neurosci. **14**(5), 732–744 (2002)

46.12 C. Tallon-Baudry, O. Bertrand, C. Delpuech, J. Pernier: Stimulus specificity of phase-locked and non-phase-locked 40 Hz visual responses in human, J. Neurosci. **16**(13), 4240–4249 (1996)

46.13 J. Wang, N. Yan, H. Liu, M. Liu, C. Tai: Brain-Computer Interfaces Based on Attention and Complex Mental Tasks, Digital Human Modeling, LNCS **4561**, 467–473 (2007)

46.14 C. Neuper, G.R. Müller, A. Kübler, N. Birbaumer, G. Pfurtscheller: Clinical application of an EEG-based brain–computer interface: A case study in a patient with severe motor impairment, Clin. Neurophysiol. **114**(3), 399–409 (2003)

46.15 D. McFarland, J.R. Wolpaw: Brain computer inerfaces for communication and cotrol, Commun. ACM **54**(5), 60–66 (2011)

46.16 L. Qin, L. Ding, B. He: Motor imagery classification by means of source analysis for brain computer interface applications, J. Neural Eng. **1**, 133–141 (2004)

46.17 B. Kamousi, Z. Liu, B. He: An EEG inverse solution based brain-computer interface, Int. J. Bioelectromagn. **7**(2), 292–294 (2005)

46.18 Q. Noirhomme, R.I. Kitney, B. Macq: Signle-trial EEG source reconstruction for brain-computer interface, IEEE Trans. Biomed. Eng. **55**(5), 1592–1601 (2008)

46.19 M. Grosse-Wentrup, C. Liefhold, K. Gramann, M. Buss: Beamforming in non-invasive brain-computer interfaces, IEEE Trans. Biomed. Eng. **56**(4), 1209–1219 (2009)

46.20 S. Choi, A. Cichocki, H.-M. Park, S.-Y. Lee: Blind source separation and independent component analysis: A review, Neural Inf. Process. **6**(1), 1–57 (2005)

46.21 P. Brasnett, L. Mihaylova, D. Bull, N. Canagarajah: Sequential Monte Carlo tracking by fusing multiple cues in video sequences, Image Vis. Comput. Elsevier Sci. **25**(8), 1217–1227 (2007)

46.22 M. Arulampalam, S. Maskell, N. Gordon, T. Clapp: A tutorial on particle filters for online nonlinear/non-Gaussian Bayesian tracking, IEEE Trans. Signal Process. **50**(2), 174–188 (2002)

46.23 J. Liu, R. Chen: Sequential Monte Carlo methods for dynamic systems, J. Am. Statist. Assoc. **93**(443), 1032–1044 (1998)

46.24 Y. Salu, L.G. Cohen, D. Rose, S. Sato, C. Kufta, M. Hallet: An improved method for localizing electric brain dipoles, IEEE Trans. Biomed. Eng. **37**, 699–705 (1990)

46.25 Y. Lai, W. Van Drongelen, L. Ding, K.E. Hecox, V.L. Towle, D.M. Frim, B. He: Estimation of in vivo human brain-skull conductivity ratio from simultaneous extra- and intra-cranial electrical potential recordings, Clin. Neurophysiol. **116**, 456–465 (2005)

46.26 J. Capon: High-resolution frequency wavenumber spectrum analysis, Proc. IEEE **57**, 1408–1418 (1969)

46.27 B.D. Van Veen, W. van Drongelen, M. Yuchtman, A. Suzuki: Localization of brain electrical activity via linearly constrained minimum variance spatial filtering, IEEE Trans. Biomed. Eng. **44**(9), 867–880 (1997)

46.28 M.-X. Huang, J.J. Shih, R.R. Lee, D.L. Harrington, R.J. Thoma, M.P. Weisend, F. Hanion, K.M. Paulson, T. Li, K. Martin, G.A. Miller, J.M. Canive: Commonalities and differences among vectorized beamformers in electromagnetic source imaging, Brain Topogr. **16**, 139–158 (2004)

46.29 H.R. Mohseni, K. Nazarpour, E.L. Wilding, S. Saeid Sanei: The application of particle filters in single trial event-related potential estimation, Physiol. Meas. **30**, 1101–1116 (2009)

46.30 H.R. Mohseni, F. Ghaderi, E.L. Wilding, S. Saeid Sanei: A beamforming particle filter for EEG dipole source localization, Int. Conf. Acoust., Speech, Signal Process. (ICASSP) (2009) pp. 337–340

46.31 J.M. Anteli, J. Mingue: EEG source localization based on dynamic Bayesian estimation techniques, Int. J. Bioelectromagn. **11**(4), 179–184 (2009)

46.32 I.M. Santos, J. Iglesias, E.I. Olivares, A.W. Young: Differential effects of object-based attention on evoked potentials to fearful and disgusted faces, Neuropsychologia **46**(5), 1468–1479 (2008)